Shahid Bahonar University of Kerman
Journal of Mahani Mathematical Research
Print ISSN: 2251-7952 Online ISSN: 2645-4505

EFFECT OF BLOOD PERFUSION ON THERMAL THERAPY IN MULTILAYER SKIN BY SEMIGROUPS APPROACH

Gh. Abbasi ✉ and S. Khishtandar

Article type: Research Article
(Received: 05 November 2023, Received in revised form 31 January 2024)
(Accepted: 25 February 2024, Published Online: 26 February 2024)

Zusammenfassung. A semi-analytical solution is proposed for the bioheat equation, which includes the epidermis, dermis, and hypodermis layers in the presence of a surface pulsed heat source. A switching time surface heating/cooling source, which has therapeutic applications in human tissue burning, is used. The interface temperature is calculated by matching the temperature and heat flux between two adjacent layers. A high-performance computing algorithm is designed and implemented by combining semigroups theory, Laplace transform, and convolution operators in each layer. It is proved that the proposed solution is consistent, convergent and stable. The reliability, performance and efficiency of semi-analytical solutions are compared using the bioheat transfer module of COMSOL software based on standard finite element methods. Numerical results for three different medical examples are given. Influences of blood pressure on temperature along the layered skin for different switching and final times are discussed.

Keywords: Abstract differential equations, Blood perfusion, Semi-analytic solution, Composite skin tissue, Pulsed heat source.
2020 MSC: 80A19, 80M10, 35Q92, 65M55, 44A10, 12H20.

1. Introduction

Although for knowing the thermal bioheat transfer in biological skin tissue the best method is to experiment, however because of the complexity in biomedical and physical processes mathematical modeling of the thermal mechanisms becomes important. The thermal human skin properties vary between three different layers: epidermis, dermis and hypodermis. Heat transfer in human skin tissue contains heat conduction (in the tissue and vascular system), convection (between tissue and blood cause to blood flow), advection (blood pressure) and diffusion (through micro-vascular beds) and metabolic heat generation [10]. In 1948, Pennes [29] established the parabolic bioheat equation (Pennes equation), in which blood pressure, metabolic thermal production and spatial heating source are imported into the classical heat equation.

There are significant amount of research on numerical solutions [2, 3, 12, 18] and semi-analytical solutions [4, 11, 24, 26] of the bioheat transfer equation in

✉ Gh.Abbasi@iau.ac.ir, ORCID: 0000-0002-0177-8557
https://doi.org/10.22103/jmmr.2024.22464.1532
Publisher: Shahid Bahonar University of Kerman
How to cite: Gh. Abbasi, S. Khishtandar, *Effect of blood perfusion on thermal therapy in multilayer skin by semigroups approach*, J. Mahani Math. Res. 2024; 13(2): 275 - 292.

a single layer tissue for different heat treatment models. In Refs. [15, 28] finite volume and finite element formulations for the bioheat equation in a model of human eye are solved. Mital and Tafreshi [27] introduced a numerical solution for the bioheat equation by finite element method to calculate an optimal thermal damage in hyperthermia cancer treatment. Malek and Abbasi [24, 26] in the years 2014 and 2016 solved several optimal boundary control problems for skin surface burning analytically by strongly continuous semigroups (C_0-semigroups) theory. In the year 2015, they derived exact solutions for the hyperbolic bioheat equation using C_0-semigroups theory along with variational methods for skin surface burning and hyperthermia cancer therapy [25].

Although there are many works on single-layer tissues, there are few works on multilayer composite live tissues. An application of the modified discretization technique and the Laplace transform to describe the thermal behavior in a living tissue is investigated by Liu et al. [19–21]. Li et al. [16] solved the governing equations in skin tissue with temperature dependent material properties by Kirchhoff and Laplace transformation. Singh et al. [32] suggested a numerical solution of the bioheat transfer model in a three-layered skin tissue freezing. The effect of blood vessels on the temperature distribution of a three-layered skin using the bioheat equation investigated numerically by Kashkooli et al. [13]. Lin and Li [17] presented a semi-analytical solution for the bioheat conduction in a three-layered skin that is subjected to heating by laser and cooling by fluid at the skin surface. The effect of air gap orientations and heterogeneous air gap in thermal protective clothing on skin burn was investigated numerically by [35]. An analytic solution for Pennes equation in a two-layer brain was derived using the Laplace transform by Ma et al. [23]. In 2019, the influence of nanoshell density on temperature using Green's function method for the bioheat equation in multilayer tissue was investigated [22]. In their study, Abbasi et al. [1] proposed a semi-analytical solution for the bioheat equation, utilizing semigroups theory and domain decomposition techniques for hyperthermia cancer treatment in layered skin tissues.

Varying blood perfusion rates in different individuals can have a significant impact on heat transfer in the multilayer human body during thermal therapy [14]. During thermal therapy, heat is applied to the body to target and destroy cancer cells or other abnormal tissue. However, the effectiveness of this treatment can be influenced by the rate of blood perfusion in the affected area. In individuals with higher blood perfusion rates, heat may be more quickly carried away from the treatment site, potentially reducing the effectiveness of the therapy. Conversely, in individuals with lower blood perfusion rates, heat may be more readily absorbed and retained in the treatment area, potentially increasing the risk of thermal damage to surrounding tissue. Moreover, the multilayer structure of the human body can further complicate the effects of varying blood perfusion rates on heat transfer [36]. Different layers of tissue may have different perfusion rates, which can lead to complex temperature gradients and heat distribution patterns throughout the body. Understanding

these patterns is crucial for optimizing the effectiveness and safety of thermal therapy. Numerous studies have explored the impact of blood perfusion on temperature distribution in the layered skin tissues for tumor therapy, using numerical methods [14, 30, 31, 36].

This paper aims to propose a semi-analytic solution for the bioheat equation with surface pulsed heat source in the context of a three-layered skin. The proposed solution simulates the effect of blood perfusion on thermal therapy. Unlike Ref. [1] when a pulsed heat source is applied, the hybrid method based on C_0-semigroups theory and the corresponding variational boundary value problem are used to derive the semi-analytical solution. The reason for using this method is that the boundary condition is a discontinuous function of time. The eigenvalue-eigenfunction formulation of infinitesimal generator for the three layers bioheat equation differs from that in Ref. [1]. The discrepancy error is addressed to quantify the difference between the exact solution and the semi-analytical solution calculated using semigroups theory. The bioheat transfer module of COMSOL Multiphysics simulation software [6] is used to validate the reliability, performance, and efficiency of a semi-analytical solution when discussing changes in blood pressure and their effect on the bioheat transfer. By regulating the surface pulsed heat source with blood perfusion rate, the therapeutic impact of tumor temperature can be optimized while minimizing damage to normal tissue. The results can be apply in clinical settings for skin burning /cooling.

The paper is organized as follows: In Section 2, the mathematical model for the three layers bioheat equation is proposed to solve the surface heating/cooling problem under specific boundary conditions. In Section 3, the C_0-semigroup formulation and closed form analytical solution for the related problem are proposed. In Section 4, the spatial state (Laplace transformation and its inversion) for the bioheat problem is put forward to determine temperatures distribution in the interface layers. In Section 5, we analyze the associated errors in the context of time and geometric errors in the semi-analytical solution. Section 6 contains three different medical work examples. In Section 7, numerical results for medical problems, including different blood flow rates and switching times, are provided. Section 8 concludes the manuscript.

2. Mathematical formulation

Here, the mathematical formulation for temperature propagation in a three-layered live skin will discuss. Figure 1 shows the schematic geometry for a surface heat source, where z_0 and z_3 denote the values for surface and body core boundaries, while z_1 and z_2 are the spatial depth values for interfaces. The thickness of the jth layer is $l_j = z_j - z_{j-1}$ for $j = 1, 2, 3$. The bioheat equation in the jth layer is governed by the partial differential equation given

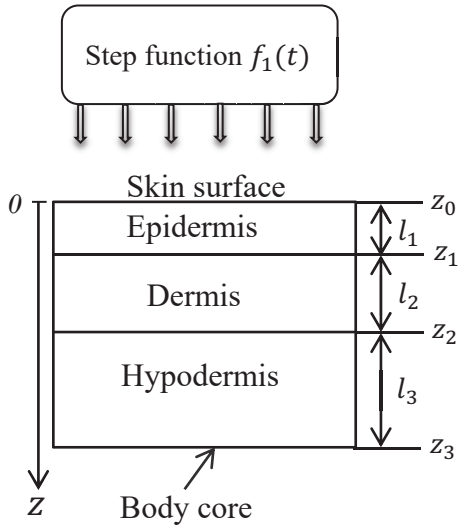

Abbildung 1. Schematic of a three-layered skin for surface burning using the step function $f_1(t)$.

by Pennes [29]:

$$\rho_j c_j \frac{\partial T_j(z,t)}{\partial t} = k_j \frac{\partial^2 T_j(z,t)}{\partial z^2} + \rho_b w_{b,j} c_b (T_b - T_j(z,t)) + q_{m,j} + q_r(z,t), \quad \text{for } (z,t) \in (z_{j-1}, z_j) \times (0, t_f),\ j = 1,2,3, \tag{1}$$

where $q_r(z,t)$ is the external environmental heat source, t is the time, t_f is the final time, T_b and $T_j(z,t)$ are the arterial and the jth layer temperature. At the jth layer c_j, k_j and ρ_j are heat capacity, thermal conductivity and density of the tissue. Here, c_b and ρ_b are heat capacity and density of the blood. Within the jth layer $q_{m,j}$ and $w_{b,j}$ are the metabolic heat source and blood pressure rate. $q_{m,j}$ is a constant value within the j layer. In the beginning time, the temperature in each layer is the same

$$T_j(z,0) = T_b, \qquad j = 1,2,3, \tag{2}$$

In this research, the aim is to investigate the effect of blood perfusion on thermal therapy while there is a pulsed heat source on the skin surface. The body core temperature was assumed to be constant, as the biological body naturally strives to maintain stability in its core temperature. Therefore, the boundary conditions for Eq. (1) are considered as follows:

$$T_1(z_0,t) = f_1(t), \quad T_3(z_3,t) = T_b, \tag{3}$$

our model uses a step function $f_1(t)$ as a pulsed heat source in thermal therapy,

where the heat is applied in pulses at specific times, as in the following

$$f_1(t) = \begin{cases} 100°\text{C} & \text{for } 0 \le t \le t_s \\ 0°\text{C} & \text{for } t_s < t \le t_f, \end{cases} \tag{4}$$

where t_s is switching time. It means that the skin surface is initially exposed to a constant-temperature heat source of 100°C, such as boiling water, at the beginning of the process ($t = 0$). After a duration of t_s seconds, the heat source is removed, and the skin is then cooled by a fluid at 0°C for a period of $(t_f - t_s)$ seconds. From continuity of the temperature and heat flux within layers $j = 2, 3$ we have [21]

$$T_{j-1}(z_{j-1}, t) = T_j(z_{j-1}, t), \tag{5a}$$

$$-k_{j-1}\frac{\partial T_{j-1}(z,t)}{\partial z} = -k_j \frac{\partial T_j(z,t)}{\partial z}, \quad \text{on } z = z_{j-1}. \tag{5b}$$

The composite skin consists of three layers: epidermis, dermis and hypodermis (subcutaneous tissue) as it is shown in Fig. 1. In the next section, we propound the novel convolution operators in each layer via semigroups theory that is useful for computing a hybrid solution for problem (1)-(5).

3. **Semigroups analysis**

Although the section focuses on a three-layered skin, it can easily extend for any multilayer composites. Let for $j = 1, 2, 3$

$$U_j(z,t) = T_j(z,t) - T_b, \tag{6}$$

by substituting (6) in (1)-(5) for $(z,t) \in (z_{j-1}, z_j) \times (0, t_f)$ and $j = 1, 2, 3$ we have

$$\rho_j c_j \frac{\partial U_j(z,t)}{\partial t} = k_j \frac{\partial^2 U_j(z,t)}{\partial z^2} - \rho_b w_{b,j} c_b U_j(z,t) + q_{m,j} + q_r(z,t), \tag{7a}$$

$$U_j(z,0) = 0, \qquad \text{for } z \in (z_{j-1}, z_j), \tag{7b}$$

$$U_1(z_0,t) = f_1(t) - T_b, \qquad U_3(z_3,t) = 0. \tag{7c}$$

Conditions in the adjacent layers yields

$$U_{j-1}(z_{j-1},t) = U_j(z_{j-1},t) \quad j = 2, 3, \tag{8a}$$

$$-k_{j-1}\frac{\partial U_{j-1}(z,t)}{\partial z} = -k_j \frac{\partial U_j(z,t)}{\partial z}, \quad \text{on } z = z_{j-1},\ j = 2, 3 \tag{8b}$$

In order to solve (7) through C_0-semigroup theory we consider

$$U_j(z,t) = W_j(z,t) + V_j(z,t), \tag{9}$$

where $W_j(z,t)$ is a function that deals with interior points in the jth layer while vanishes at the boundaries and $V_j(z,t)$ deals with boundary conditions altogether with interface conditions. To do so let

$$V_j(z,t) = \frac{1}{l_j}\Big((z_j - z)U_j(z_{j-1},t) + (z - z_{j-1})U_j(z_j,t)\Big). \tag{10}$$

Thus, from Eqs. (7)-(10) one can write

$$\frac{\partial W_j(z,t)}{\partial t} = \frac{k_j}{\rho_j c_j}\frac{\partial^2 W_j(z,t)}{\partial z^2} - \frac{\rho_b w_{b,j} c_b}{\rho_j c_j} W_j(z,t) + \frac{1}{\rho_j c_j} q_r(z,t)$$

$$+ \frac{1}{\rho_j c_j}\Big(q_{m,j} - \rho_b w_{b,j} c_b V_j(z,t)\Big) - \frac{\partial V_j(z,t)}{\partial t}, \tag{11a}$$

$$W_j(z,0) = -V_j(z,0), \qquad \text{for } z \in (z_{j-1}, z_j),\ j = 1,2,3, \tag{11b}$$

$$W_1(z_0,t) = 0, \quad W_3(z_3,t) = 0. \tag{11c}$$

We describe problem (11) as an infinite dimensional inhomogeneous abstract differential equation [25],

$$\frac{\mathrm{d}\mathbf{W}(t)}{\mathrm{d}t} = \mathbf{A}\mathbf{W}(t) + \mathbf{B}\, q_r(z,t) + \mathbf{F}(t), \ \ t \geq 0, \ \ \mathbf{W}(0) = -\mathbf{V}(0), \tag{12}$$

where $\mathbf{F}(t) = \big(f_1(z,t)\ f_2(z,t)\ f_3(z,t)\big)^\top$ for $f_j(z,t) = \frac{1}{\rho_j c_j}\big(q_{m,j} - \rho_b w_{b,j} c_b V_j(z,t)\big) - \frac{\partial V_j(z,t)}{\partial t}$ and $\mathbf{V}(0) = \big(V_1(z,0)\ V_2(z,0)\ V_3(z,0)\big)^\top$, in which $\mathbf{A}$ is a diagonal matrix

$$\mathbf{A} = \mathrm{diag}\,\big(A_1, A_2, A_3\big) \text{ such that } A_j = \frac{1}{\rho_j c_j}\Big(k_j \frac{\mathrm{d}^2}{\mathrm{d}z^2} - \rho_b w_{b,j} c_b\Big). \tag{13}$$

Here, $\mathbf{W}(t) = \big(W_1(z,t)\ W_2(z,t)\ W_3(z,t)\big)^\top$ is state, the function $q_r(z,t)$ is input function and $\mathbf{B} = \big(\frac{1}{\rho_1 c_1}\ \frac{1}{\rho_2 c_2}\ \frac{1}{\rho_3 c_3}\big)^\top$ is an input operator. We choose the Hilbert space $H = L^2([z_0, z_1]) \times L^2([z_1, z_2]) \times L^2([z_2, z_3])$ as the state space equipped with inner product

$$\langle \mathbf{U}, \mathbf{W}\rangle_H = \sum_{j=1}^{3} \langle U_j, W_j\rangle_{L^2([z_{j-1}, z_j])}, \text{ for } \mathbf{U}, \mathbf{W} \in H, \tag{14}$$

where $\mathbf{U}(t) = \big(U_1(z,t)\ U_2(z,t)\ U_3(z,t)\big)^\top$ and we assume that $\mathbf{W}(0) \in H$. The symbol $\langle ., . \rangle_{L^2([z_{j-1}, z_j])}$ shows inner product for the space $L^2([z_{j-1}, z_j])$ of square-integrable functions defined on the interval $[z_{j-1}, z_j]$, which defined as

$$\langle U_j, W_j\rangle_{L^2([z_{j-1}, z_j])} = \int_{z_{j-1}}^{z_j} U_j(z,t) \times W_j(z,t)\, dz \ \text{ for } \ U_j, W_j \in L^2([z_{j-1}, z_j])$$

In the remainder of this section, the infinite dimensional linear system theories introduced in Ref. [7] are applied to the multilayer bioheat equation (11). In the next theorem, it is shown that there exists a strongly continuous semigroup with infinitesimal generator $\mathbf{A}$ as it is defined in (13).

Theorem 3.1. *If domain of A_j for $j = 1, 2, 3$ given by* (13) *has the following properties:*

$$\boldsymbol{D}(A_j) = \Big\{ W_j(.,t) \in \boldsymbol{L}_2[z_{j-1}, z_j] \Big| \, W_j \text{ and } \frac{\mathrm{d}W_j}{\mathrm{d}z} \text{ are absolutely continuous,} \tag{15}$$
$$\frac{\mathrm{d}^2 W_j}{\mathrm{d}z^2} \in \boldsymbol{L}_2[z_{j-1}, z_j] \text{ and } W_j \text{ vanishes at } j\text{th layer interface and boundary} \Big\},$$

then problem (12) *forms an inhomogeneous abstract differential equation.*

Beweis. The proof is based on the extension for Theorem 2.2.2 in Ref. [7] using domain decomposition techniques. □

Theorem 3.2. *For $j = 1, 2, 3$ and n belonging to the set of natural numbers on the interval $[z_{j-1}, z_j]$, the eigenvalues for the operator A_j with the properties in Theorem 3.1 are*

$$\lambda_{n,j} = -\frac{\rho_b w_{b,j} c_b + k_j p_{n,j}^2}{\rho_j c_j}, \tag{16}$$

where in each layer $p_{n,j}$ is

$$p_{n,j} = \frac{n\pi}{z_j - z_{j-1}}. \tag{17}$$

Moreover, corresponding eigenfunctions are

$$\phi_{n,j}(z) = \sqrt{\frac{2}{z_j - z_{j-1}}} \sin(p_{n,j}(z - z_{j-1})), \quad z \in [z_{j-1}, z_j], \; n = 1, 2, \ldots. \tag{18}$$

Beweis. According to (13) the eigenvalue-eignfunction problem $A_j \phi_{n,j} = \lambda_{n,j} \phi_{n,j}$ is equivalent to

$$\frac{1}{\rho_j c_j} \Big(k_j \frac{\mathrm{d}^2 \phi_{n,j}}{\mathrm{d}z^2} - \rho_b w_{b,j} c_b \phi_{n,j} \Big) = \lambda_{n,j} \phi_{n,j}. \tag{19}$$

The sequence $\{\phi_{n,j}(z)\}_{n=1}^{\infty}$ in (18), form an orthonormal basis on $L^2([z_{j-1}, z_j])$. Substituting basis (18) in Eq. (19) proves the theorem. □

In the next theorem, we show the relation of each layer's semigroup with the overall semigroup for the entire geometry.

Theorem 3.3. *If each A_j for $j = 1, 2, 3$ is the infinitesimal generator of a C_0-semigroup $(S_j(t))_{t \geq 0}$, then the operator $\mathbf{A}$ in* (13) *is the infinitesimal generator of a C_0-semigroup $(\mathbf{S}(t))_{t \geq 0}$ on H defined as*

$$\mathbf{S}(t) = \operatorname{diag}\big(S_1(t), S_2(t), S_3(t)\big). \tag{20}$$

Beweis. For $j = 1, 2, 3$ and $n = 1, 2, \cdots$, from the Hille–Yosida Theorem [7] since $\lambda_{n,j} < 0$ (see Eq. (16)), then the operator A_j is the infinitesimal generator for a C_0-semigroup $(S_j(t))_{t\geq 0}$ on $L^2([z_{j-1}, z_j])$ defined as

$$S_j(t)W_j = \sum_{n=1}^{\infty} e^{\lambda_{n,j}t}\langle W_j, \phi_{n,j}\rangle\phi_{n,j}(z). \tag{21}$$

i.e., the operator A_j generates the unique C_0-semigroup $(S_j(t))_{t\geq 0}$. This proves the theorem. □

Conditions for problem (11) under which closed form analytical solution $W_j(z,t)$ exists are given in the following theorem.

Theorem 3.4. *If* $q_r(z,t) \in \boldsymbol{L}_2([0,t_f],\mathbb{R})$, *then* $\mathbf{W}(t) = \big(W_1(z,t)\ W_2(z,t)\ W_3(z,t)\big)^\top$ *is a unique mild solution for inhomogeneous abstract differential equation* (12) *where for* $j = 1, 2, 3$, *we have*

$$\begin{aligned} W_j(z,t) &= \sum_{n=1}^{\infty} e^{\lambda_{n,j}t}\big\langle -V_j(\xi,0), \phi_{n,j}(\xi)\big\rangle\phi_{n,j}(z) \\ &+ \frac{1}{\rho_j c_j}\sum_{n=1}^{\infty}\int_0^t e^{\lambda_{n,j}(t-s)}\big\langle q_{m,j} + q_r(\xi,s), \phi_{n,j}(\xi)\big\rangle\,\mathrm{d}s\,\phi_{n,j}(z) \\ &- \frac{\rho_b w_{b,j} c_b}{\rho_j c_j}\sum_{n=1}^{\infty}\int_0^t e^{\lambda_{n,j}(t-s)}\big\langle V_j(\xi,s), \phi_{n,j}(\xi)\big\rangle\,\mathrm{d}s\,\phi_{n,j}(z) \\ &- \sum_{n=1}^{\infty}\int_0^t e^{\lambda_{n,j}(t-s)}\Big\langle \frac{\partial V_j(\xi,s)}{\partial s}, \phi_{n,j}(\xi)\Big\rangle\,\mathrm{d}s\,\phi_{n,j}(z). \end{aligned} \tag{22}$$

Beweis. Theorem 4 in Ref. [25] yields

$$\mathbf{W}(t) = \mathbf{S}(t)\{-\mathbf{V}(0)\} + \int_0^t \mathbf{S}(t-s)\{\mathbf{B}q_r(z,s) + \mathbf{F}(s)\}\,\mathrm{d}s. \tag{23}$$

Thus, from (12), and by substituting (20) into (23), the theorem can be proved. □

Up to now, the interface functions $U_1(z_1,t)$, $U_2(z_1,t)$, $U_2(z_2,t)$, and $U_3(z_2,t)$ in (10) are four unknown functions. From continuity conditions (8a), we have two unknown interface functions, i.e., $U_1(z_1,t) = U_2(z_1,t)$ and $U_2(z_2,t) = U_3(z_2,t)$. The corresponding steady unknown interface functions are $\widetilde{U}_1(z_1,s)$ and $\widetilde{U}_2(z_2,s)$, which can be determined by Laplace transformation on $W_j(z,t)$ for $j = 1, 2, 3$, and by matching the first derivative conditions (8b) at the two interfaces. Now, the numerical Laplace inversion on $\widetilde{W}_j(z,s)$ for $j = 1, 2, 3$ gives an approximate solution $u_j(z,t)$ for $U_j(z,t) = W_j(z,t) + V_j(z,t)$.

4. Semi-analytical solution

Here, the solution (22) is mapped to steady function $\widetilde{W}_j(z,s)$ by the Laplace transform where s is the Laplace transformation parameter. Using the convolution integral theorem [5] and applying the Laplace transform to Eq. (22) yields

$$\begin{aligned}\widetilde{W}_j(z,s) = &\frac{1}{\rho_j c_j}\sum_{n=1}^{\infty}\frac{1}{s-\lambda_{n,j}}\Big\langle \frac{q_{m,j}}{s} + \widetilde{q}_r(\xi,s), \phi_{n,j}(\xi)\Big\rangle \phi_{n,j}(z)\\ &- \Big(s + \frac{\rho_b w_{b,j} c_b}{\rho_j c_j}\Big)\sum_{n=1}^{\infty}\frac{1}{s-\lambda_{n,j}}\langle \widetilde{V}_j(\xi,s), \phi_{n,j}(\xi)\rangle \phi_{n,j}(z).\end{aligned} \tag{24}$$

Thus, we have

$$\widetilde{U}_j(z,t) = \widetilde{W}_j(z,t) + \widetilde{V}_j(z,t). \tag{25}$$

Now, the Laplace transformation in conjunction with Eqs. (8a) and (8b) for boundary conditions at the interfaces of two adjacent layers yields

$$\widetilde{U}_{j-1}(z_{j-1},s) = \widetilde{U}_j(z_{j-1},s), \qquad j=2,3, \tag{26a}$$

$$-k_{j-1}\frac{\partial \widetilde{U}_{j-1}(z,s)}{\partial z} = -k_j \frac{\partial \widetilde{U}_j(z,s)}{\partial z}, \qquad \text{on } z=z_{j-1},\ j=2,3. \tag{26b}$$

Substituting Eqs. (25) and (26a) into Eq. (26b) can produce a system of two linear equations in two unknowns steady functions $\widetilde{U}_j(z_j,s)$. In conjunction with Eq. (6) one can write the steady temperature

$$\widetilde{T}_j(z,s) = \widetilde{U}_j(z,s) + T_b/s. \tag{27}$$

However, at the interfaces, taking analytical inverse Laplace transform from Eq. (27) is complicated [21]. For this reason, authors compute $\widetilde{U}_j(z,s)$ and hence $\widetilde{T}_j(z,s)$ for $j=1,2,3$ by a numerical Laplace inversion based on Dubner and Abate's method [8]. It is obvious that at this stage, we have a semi-analytical solution that needs to be validated.

5. Error bound and stability analysis

Theoretical validation is done by error analysis of geometric, time, and discretization errors as discrepancy error.

5.1. **Geometric error.** Geometric error results from the error associated with the truncation of series solution (22) by first M_s terms. In order to compute the approximate solution $u_j(z,t)$ for $j=1,2,3$ one must truncate (22) at some order, say $n=M_s$ to obtain an approximate solution $u_j(z,t)$. Thus, we have a geometric error $E_s(z,t;M_s) = U_j(z,t) - u_j(z,t)$ as

$$|E_s(z,t;M_s)| \le |E_s(z,0;M_s)| = \sum_{n=M_s+1}^{\infty}\langle -V_j(\xi,0), \phi_{n,j}(\xi)\rangle \phi_{n,j}. \tag{28}$$

From (10) and (28), one can calculate that for $M_s = 25$, the geometric error vanishes using the best approximation theorem (See page 197 of Ref. [34]).

5.2. **Time error.** Here, for N_t as a finite integer number, the numerical Laplace inversion method in Eq. (24) is based on the Fourier series expansion developed by Durbin [8] as

$$W_j^{N_t}(z,t) = \frac{e^{\upsilon t}}{P}\Big[\frac{-1}{2}\operatorname{Re}(\widetilde{W}_j(z,\upsilon)) + \sum_{k=0}^{N_t}\operatorname{Re}\big(\widetilde{W}_j(z,\upsilon+i\frac{k\pi}{P})\big)\cos(\frac{k\pi}{P}t) - \operatorname{Im}\big(\widetilde{W}_j(z,\upsilon+i\frac{k\pi}{P})\big)\sin(\frac{k\pi}{P}t)\Big], \tag{29}$$

Here, $\upsilon \in \mathbb{R}$ and $t \in [0, 2P]$, where $2P$ represents the nonzero constant period of the function $\widetilde{W}_j$. Thus, one will encounter the time error

$$E_t(N_t,\upsilon,t,P) = \frac{e^{\upsilon t}}{P}\Big[\sum_{k=N_t+1}^{\infty}\operatorname{Re}\big(\widetilde{W}_j(z,\upsilon+i\frac{k\pi}{P})\big)\cos(\frac{k\pi}{P}t) - \operatorname{Im}\big(\widetilde{W}_j(z,\upsilon+i\frac{k\pi}{P})\big)\sin(\frac{k\pi}{P}t)\Big], \tag{30}$$

while the discretization error is

$$E_d(\upsilon,t,P) = \sum_{k=1}^{\infty} e^{-2\upsilon kP} W_j(z, 2kP+t). \tag{31}$$

The integer N_t can be determined from (30) and (31) using the series convergence criterion: $|\operatorname{Re}(\widetilde{W}_j(z,\upsilon+iN_t\frac{2\pi}{P}))|$ and $|\operatorname{Im}(\widetilde{W}_j(z,\upsilon+iN_t\frac{2\pi}{P}))| \le \frac{\varepsilon P}{\exp(\upsilon P)}$ for $\varepsilon = 10^{-6}$ to 10^{-10}. Durbin found that υP in the range 5 to 10 yielded satisfactory results for N_t ranging from 50 to 5000 [8]. In this manuscript, results are presented for $N_t = 2000$, implying that both time and discretization errors diminish as $N_t \to 2000$.

5.3. **Discrepancy error.** In the following, we use the discrepancy error to prove the consistency, convergence, and stability of the semi-analytical solution. Let $L(\mathbf{U}) = \mathbf{0}$ represent the system of partial differential equations (7) in the independent variable z and t, with an exact solution $\mathbf{U} = (U_1\ U_2\ U_3)^\top$ where $U_j(z,t) = W_j(z,t) + V_j(z,t)$ for $j = 1,2,3$ (see Eqs. (10) and (22)).

We assume that $F_{M_s\,N_t}(\mathbf{u}) = \mathbf{0}$ represents the approximating system based on semigroup and Laplace transform techniques, with a semi-analytical solution $\mathbf{u} = (u_1\ u_2\ u_3)^\top$ where u_j is the approximate solution for U_j; $j = 1,2,3$. Then

$$\mathbf{e} = \begin{pmatrix} e_1 & e_2 & e_3 \end{pmatrix}^\top = \mathbf{U} - \mathbf{u}. \tag{32}$$

Note that the difference between $U_j(z,t)$ and $u_j(z,t)$ in our mathematical model can arise from the geometric error, time error, and discretization error. The geometric error occurs when calculating the summation in the first M_s terms of (22), while the time and discretization errors occur when we apply numerical Laplace inversion.

TABELLE 1. Available properties for three-layered live skin tissue used in numerical computations [21].

Parameters	Blood	Epidermis	Dermis	Hypodermis
c_j (J/kg °C)	3770.0	3600.0	3300.0	2700.0
ρ_j (kg/m^3)	1060.0	1190.0	1116.0	971.0
k_j (W/m °C)	-	0.235	0.445	0.185
$q_{m,j}$ (Wm^{-3})	-	368.1	368.1	368.3
l_j (m)	-	0.0001	0.0015	0.0044

Let ν be a continuous function of z and t with a sufficient number of continuous derivatives to enable the evaluation of $L(\nu)$ in $[0, l] \times [0, 2P]$. Now, by proposing the discrepancy error

$$D(\nu) = F_{M_s\, N_t}(\nu) - L(\nu), \tag{33}$$

we discuss the consistency. Since most authors may put $\nu = U$, because $L(\mathbf{U}) = 0$, it then follows that $D(\mathbf{U}) = F_{M_s\, N_t}(\mathbf{U})$. Thus, from Subsections 5.1 and 5.2 for $M_s \geq 25$ and $2000 \leq N_t \leq 5000$, we have the approximate solution $\mathbf{u} \to \mathbf{U}$. Hence, from Eq. (32) we have $\mathbf{e} \to \mathbf{0}$, thus $D(\mathbf{U}) \to \mathbf{0}$. This idea proposes a conditional compatibility or consistency between the model used in computation and the model used to simulate the system. From Eq. (21), the model is stable for $\lambda_{n,j} < 0$ (see Eq. (16)). Thus, from Lax theorem [33], semi-analytical solution u_j converges to exact solution U_j.

In the next section, three different cases are solved to show the efficiency of proposed hybrid method given in Sections 3 and 4. Semi-analytical solutions for the problem of surface burning in Section 2 are calculated and the corresponding graphs are depicted to show the practicality and efficiency of this technique in medical thermal therapy in the presence of a surface pulsed heat source.

6. **Work examples**

Applications of this study can be found in bio-engineering science in skin tissue, the temperature effect on human blood perfusion, skin burning due to a flash fire, hot plate, liquid and gas and atomic explosion, respectively [21]. Blood perfusion is one of the important factors affecting the thermal response in living tissues. Therefore, we solve the problem of bioheat transfer given by (1)-(5) for three layers of epidermis, dermis and hypodermis (see Fig. 1), to investigate effect of blood perfusion on thermal therapy in human skin. Blood perfusion is exclusively taken into account within the dermis layer, whereas metabolic heat source is considered in all three layers. We present the following three different cases using thermophysical properties of live skin listed in Table 1.

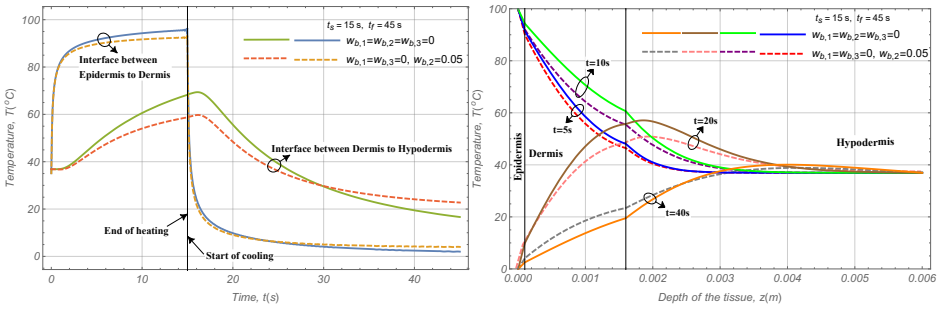

(A) (B)

ABBILDUNG 2. For switching time $t_s = 15$s and final time $t_f = 45$s when blood perfusion rates are $w_{b,2} = 0$ m^3/m^{3}s and $w_{b,2} = 0.05$ m^3/m^{3}s in the dermis layer (a) Temperature response versus time at two different layer interfaces: Epidermis-Dermis and Dermis-Hypodermis. (b) Effect of blood perfusion on the temperature response along layered skin depth for t =5s, 10s, 20s and 40s.

Case i. (*No blood perfusion*) Lets $w_{b,1} = w_{b,2} = w_{b,3} = 0$ m^3/m^{3}s, this might happen when one faces no blood perfusion in the live skin.

Case ii. (*Moderate blood perfusion*) Lets $w_{b,1} = w_{b,3} = 0$ m^3/m^{3}s and $w_{b,2} = 0.025$ m^3/m^{3}s. Here, it is assumed that the blood perfusion that is only considered in dermis layer [21].

Case iii. (*High blood perfusion*) Lets $w_{b,1} = w_{b,3} = 0$ m^3/m^{3}s and $w_{b,2} = 0.05$ m^3/m^{3}s. In this case, the temperature profile in tissue depth for higher blood perfusion in dermis layer is investigated.

For **Cases i** and **iii**, the temperature response in the three-layered skin with respect to changes in blood perfusion is considered, while surface step function (4) is applied for the heating period of time $0 \leq t \leq t_s$ and the cooling period of time $t_s \leq t \leq t_f$ respectively. In **Case ii**, the effect of surface step function (4) on the temperature response is investigated for moderate perfusion as time passes.

The steady temperature $\widetilde{T}_j(z, s)$ in (27) is computed using the first 25 terms of Eq. (24), i.e., $M_s = 25$. Moreover, we assume that the arterial blood temperature is uniform throughout the tissue and is taken as body temperature, with a value of $T_b = 37°$C. Without loss of generality, we also assume that there is no external environmental heat source in our model, i.e., $q_r(z, t) = 0$. In the next section, we will present the results and discussions related to the implementation of numerical and semi-analytical methods on the work examples.

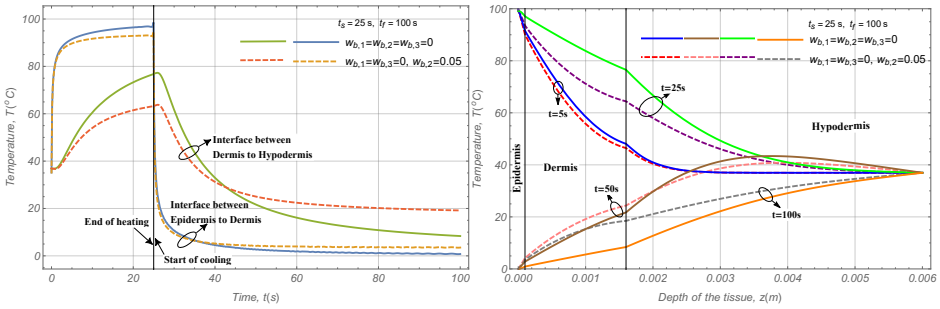

(A) (B)

ABBILDUNG 3. For switching time $t_s = 25$s and final time $t_f = 100$s, when the blood perfusion rates are $w_{b,2} = 0$ m^3/m^3s and $w_{b,2} = 0.05$ m^3/m^3s in the dermis layer (a) Temperature response versus time at two different layer interfaces: Epidermis-Dermis and Dermis-Hypodermis. (b) Effect of blood perfusion on the temperature response along layered skin depth for $t = 5$s, 25s, 50s and 100s.

7. Results and discussions

In clinical settings, we often want to predict the thermal response for different switching times t_s and final time t_f. Thus, we investigate the temperature response for $t_s = 15$s and $t_f = 45$s, as well as for $t_s = 25$s and $t_f = 100$s. In both cases, we examine medical case examples from Section 6 based on the proposed hybrid method in Sections 3 and 4, as well as the mathematical model in Section 2 for surface burning.

Figure 2 presents the results for the perfuse rates for **Cases i**: $w_{b,1} = w_{b,2} = w_{b,3} = 0$ m^3/m^3s and **Case iii**: $w_{b,1} = w_{b,3} = 0$ m^3/m^3s and $w_{b,2} = 0.05$ m^3/m^3s when switching time $t_s = 15$s and final time $t_f = 45$s. Figure 3 shows the effect of blood perfusion on the temperature response when a surface step function (4) is applied for the switching time $t_s = 25$s and final time $t_f = 100$s. As expected, when the penetration depth of the thermal signal increases, the temperature response curves will be smoother. Figures 2(a) and 3(a) show that the highest temperature increase appears at the end of heating (time t_s). Figure 2(b) presents temperature response in the skin depth during the heating period (for fixed times t =5s and 10s) or the cooling period (for fixed times t =20s and t =40s). The results from Figs. 2 and 3 are important for selecting an appropriate heating plan when estimating the blood perfusion, switching time or some other thermal parameters.

In Eq. (1), the perfusion term $\rho_b w_{b,j} c_b (T_b - T_j(z,t))$ represents the temperature exchanged between the blood and the skin. When $T_j < T_b$, the arterial

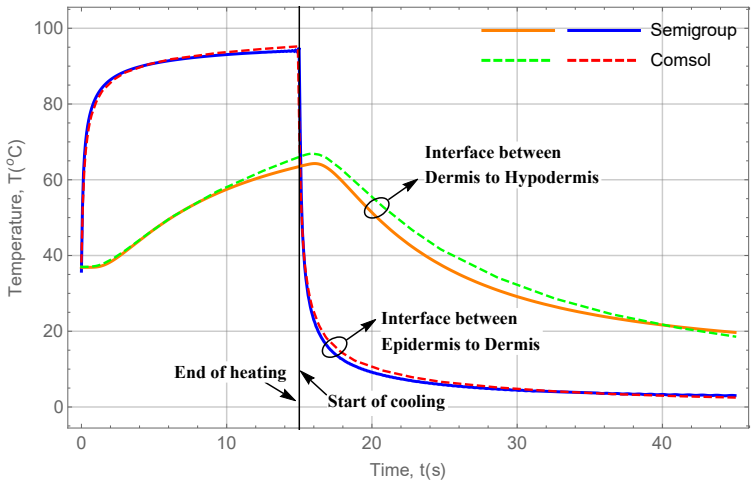

ABBILDUNG 4. Temperatures at two interfaces compared, using the COMSOL software and proposed semi-analytical solution for switching time $t_s = 15$s, final time $t_f = 45$s and blood perfusion rate $w_{b,2} = 0.025$ m^3/m^{3}s in the dermis.

blood acts as a heat source, while when $T_j > T_b$, it acts as a heat sink. In our example, during the heating period, heat loss is facilitated via the blood perfusion when t=5s and 10s, while the arterial blood functions as a heat source at $t = 40$s (see Fig. 2(b)). At t =20s the situation is different from times $t = 5$s, 10s and 40s, as dissipating the accumulated heat in the skin requires some time when there is no blood perfusion. When $w_{b,1} = w_{b,2} = w_{b,3} = 0$ m^3/m^{3}s the skin temperature is higher than when we have $w_{b,1} = w_{b,3} = 0$ m^3/m^{3}s and $w_{b,2} = 0.05$ m^3/m^{3}s. A similar procedure can be observed for the temperature response in Figure 3(b).

In Figure 4 numerical simulations based on the finite element method [9] using COMSOL Multiphysics software [6] are conducted to compare the semi-analytical solutions for switching time $t_s = 15$s, final time $t_f = 45$s and blood perfusion rate $w_{b,2} = 0.025$ m^3/m^{3}s in the dermis layer. The implemented model uses the bioheat transfer module for the Fourier model in COMSOL software and the boundary conditions were selected according to what was mentioned in the semi-analytical method (see Section 2). All of the simulations have been conducted using a 2.8 GHz Intel Core i7 CPU 11th Generation with 16 GB RAM. We have a computational time of less than 40 s for each simulation.

8. Conclusions

The transfer of heat in living tissue is significantly influenced by blood perfusion and has numerous applications in medical treatments. Therefore, accurate

temperature predictions in human skin are useful for improving the effect of blood perfusion on thermal response. The conclusions here are threefold. First, the current semi-analytical solution for investigating the behavior of bioheat transfer in three-layered skin tissue with the bioheat governing equation works well. Second, conditions for consistency and stability are determined, and convergent results are provided for those conditions. Third, the blood perfusion effect on thermal therapy is simulated via the semi-analytic solution, demonstrating its efficiency. The semi-analytic solution, based on strongly continuous semigroups theory and domain decomposition technique, is then compared with the finite element scheme using COMSOL Multiphysics software. The results coincide with the published literature concerning the surface heating approach. Although part of the idea in this paper is followed for the thermal propagation of bioheat transfer in a three-layered skin, it is possible, based on the authors' knowledge, to apply this idea for computation heat distribution in various types of multilayer composites under surface heating.

Acknowledgments

The authors would like to thank the anonymous reviewers for their valuable comments and suggestions which greatly enhance the quality of this manuscript.

Declarations

Conflict of interest The authors declare that the publication of this paper has no conflict of interest.

Literatur

[1] Abbasi, GH., & Malek, A. (2019). Hyperthermia cancer therapy by domain decomposition methods using strongly continuous semigroups. *Mathematics and Computers in Simulation*, **165**, 1–12. https://doi.org/10.1016/j.matcom.2019.02.015

[2] Akula, S. C., & Maniyeri, R. (2020). Numerical simulation of bioheat transfer: a comparative study on hyperbolic and parabolic heat conduction. *Journal of the Brazilian Society of Mechanical Sciences and Engineering*, **42**(62), 1–13. https://doi.org/10.1007/s40430-019-2132-x

[3] Al-Humedi, H. O., & Al-Saadawi, F. A. (2021). The numerical solution of bioheat equation based on shifted Legendre polynomial. *International Journal of Nonlinear Analysis and Applications*, **12**(2), 1061–1070. https://doi.org/10.22075/ijnaa.2021.5175

[4] Askarizadeh, H., & Ahmadikia, H. (2015). Analytical study on the transient heating of a two-dimensional skin tissue using parabolic and hyperbolic bioheat transfer equations. *Applied Mathematical Modelling*, **39**(13), 3704–3720. https://doi.org/10.1016/j.apm.2014.12.003

[5] Boyce, W. E., DiPrima, R. C., & Meade, D. B. (1992). *Elementary differential equations and boundary value problems* (Vol. 9). New York: Wiley.

[6] COMSOL Modeling Software. (2023). *COMSOL Multiphysics version: 6.2*. Burlington, MA, United States: COMSOL Inc. https://www.comsol.com

[7] Curtain, R. F., & Zwart, H. (1995). *An introduction to infinite-dimensional linear systems theory* (Vol. 21). New York: Springer-Verlag.

[8] Durbin, F. (1974). Numerical inversion of Laplace transforms: an efficient improvement to Dubner and Abate's method. *The Computer Journal*, **17**(4), 371–376. https://doi.org/10.1093/comjnl/17.4.371

[9] Finite Element Method. (2017). COMSOL Multiphysics Cyclopedia. https://www.comsol.com/multiphysics/finite-element-method

[10] Hobiny, A. D., & Abbas, I. A. (2018). Theoretical analysis of thermal damages in skin tissue induced by intense moving heat source. *International Journal of Heat and Mass Transfer*, **124**, 1011–1014. https://doi.org/10.1016/j.ijheatmasstransfer.2018.04.018

[11] Hooshmand, P., Moradi, A., & Khezry, B. (2015). Bioheat transfer analysis of biological tissues induced by laser irradiation. *International Journal of Thermal Sciences*, **90**, 214–223. https://doi.org/10.1016/j.ijthermalsci.2014.12.004

[12] Kalateh Bojdi, Z., & Askari Hemmat, A. (2017). Wavelet collocation methods for solving the Pennes bioheat transfer equation. *Optik*, **130**, 345–355. https://doi.org/10.1016/j.ijleo.2016.10.102

[13] Kashcooli, M., Salimpour, M. R., & Shirani, E. (2017). Heat transfer analysis of skin during thermal therapy using thermal wave equation. *Journal of Thermal Biology*, **64**, 7–18. https://doi.org/10.1016/j.jtherbio.2016.12.007

[14] Kazemi Alamouti, A., Habibi, M. R., Mazidi Sharfabadi, M., & Akbari Lalimi, H. (2021). Numerical study on the effects of blood perfusion and tumor metabolism on tumor temperature for targeted hyperthermia considering a realistic geometrical model of head layers using the finite element method. *SN Applied Sciences*, **3**(462), 1–17. https://doi.org/10.1007/s42452-021-04447-1

[15] Li, E., Liu, G. R., Tan, V., & He, Z. C. (2010). Modeling and simulation of bioheat transfer in the human eye using the 3D alpha finite element method (αFEM). *International Journal for Numerical Methods in Biomedical Engineering*, **26**(8), 955–976. https://doi.org/10.1002/cnm.1372

[16] Li, X., Li, C., Xue, Z., & Tian, X. (2018). Analytical study of transient thermo-mechanical responses of dual-layer skin tissue with variable thermal material properties. *International Journal of Thermal Sciences*, **124**, 459–466. https://doi.org/10.1016/j.ijthermalsci.2017.11.002

[17] Lin, S. M., & Li, C. Y. (2017). Semi-analytical solution of bio-heat conduction for multilayers skin subjected to laser heating and fluid cooling. *Journal of Mechanics in Medicine and Biology*, **17**(2), 1750029–25. https://doi.org/10.1142/s0219519417500294

[18] Liu, K. C., & Chen, H. T. (2015). Analysis of the bioheat transfer problem with pulse boundary heat flux using a generalized dual-phase-lag model. *International Communications in Heat and Mass Transfer*, **65**, 31–36. https://doi.org/10.1016/j.icheatmasstransfer.2015.04.004

[19] Liu, K. C., & Chen, T. M. (2018). Analysis of the thermal response and requirement for power dissipation in magnetic hyperthermia with the effect of blood temperature. *International Journal of Heat and Mass Transfer*, **126**, 1048–1056. https://doi.org/10.1016/j.ijheatmasstransfer.2018.06.024

[20] Liu, K. C., & Chen, Y. S. (2016). Analysis of heat transfer and burn damage in a laser irradiated living tissue with the generalized dual-phase-lag model. *International Journal of Thermal Sciences*, **103**, 1–9. https://doi.org/10.1016/j.ijthermalsci.2015.12.005

[21] Liu, K. C., Wang, Y. N., & Chen, Y. S. (2012). Investigation on the bio-heat transfer with the dual-phase-lag effect. *International Journal of Thermal Sciences*, **58**, 29–35. https://doi.org/10.1016/j.ijthermalsci.2012.02.026

[22] Ma, J., Yang, X., Sun, Y., Yang, J., & Yu, J. (2019). Theoretical analysis of nanoshell-assisted thermal treatment for subcutaneous tumor. *Journal of The Mechanical Behavior of Biomedical Materials*, **93**, 70–80. https://doi.org/10.1016/j.jmbbm.2019.01.016

[23] Ma, W., Liu, W., & Li, M. (2016). Analytical heat transfer model for targeted brain hypothermia. *International Journal of Thermal Sciences*, **100**, 66–74. https://doi.org/10.1016/j.ijthermalsci.2015.09.014

[24] Malek, A. & Abbasi, GH. (2014). Optimal control solution for Pennes' equation using strongly continuous semigroup. *Kybernetika*, **50**(4), 530–543. https://doi.org/10.14736/kyb-2014-4-0530

[25] Malek, A., & Abbasi, G. (2015). Heat treatment modelling using strongly continuous semigroups. *Computers in Biology and Medicine*, **62**, 65–75. https://doi.org/10.1016/j.compbiomed.2015.03.030

[26] Malek, A., & Abbasi, GH. (2016). Optimal control for Pennes' bioheat equation. *Asian Journal Of Control*, **18**(2), 674–685. https://doi.org/10.1002/asjc.1059

[27] Mital, M., & Tafreshi, H. V. (2012). A methodology for determining optimal thermal damage in magnetic nanoparticle hyperthermia cancer treatment. *International Journal for Numerical Methods in Biomedical Engineering*, **28**(2), 205–213. https://doi.org/10.1002/cnm.1456

[28] Narasimhan, A., & Jha, K. K. (2012). Bio-heat transfer simulation of retinal laser irradiation. *International Journal for Numerical Methods in Biomedical Engineering*, **28**(5), 547–559. https://doi.org/10.1002/cnm.1489

[29] Pennes, H. H. (1998). Analysis of tissue and arterial blood temperatures in the resting human forearm. *Journal of Applied Physiology*, **85**(1), 5–34. https://doi.org/10.1152/jappl.1998.85.1.5

[30] Saiko, G. (2022). Skin temperature: the impact of perfusion, epidermis thickness, and skin wetness. *Applied Sciences*, **12**(14), 7106–7120. https://doi.org/10.3390/app12147106

[31] Shirkavand, A., & Nazif, H. R. (2019). Numerical study on the effects of blood perfusion and body metabolism on the temperature profile of human forearm in hyperthermia conditions. *Journal of Thermal Biology*, **84**, 339–350. https://doi.org/10.1016/j.jtherbio.2019.07.023

[32] Singh, S., & Kumar, S. (2014). Numerical study on triple layer skin tissue freezing using dual phase lag bio-heat model. *International Journal of Thermal Sciences*, **86**, 12–20. https://doi.org/10.1016/j.ijthermalsci.2014.06.027

[33] Smith, G. D. (1985). *Numerical solution of partial differential equations: finite difference methods*. United Kingdom: Clarendon Press.

[34] Stade, E. (2011). *Fourier analysis* (Vol. 109). Germany: Wiley.

[35] Udayraj, Talukdar, P., Das, A. & Alagirusamy, R. (2017). Numerical investigation of the effect of air gap orientations and heterogeneous air gap in thermal protective clothing on skin burn. *International Journal of Thermal Sciences*, **121**, 313–321. https://doi.org/10.1016/j.ijthermalsci.2017.07.025

[36] Wahyudi, S., Vardiansyah, N. R., & Setyorini, P. H. (2022). Effect of blood perfusion on temperature distribution in the multilayer of the human body with interstitial hyperthermia treatment for tumour therapy. *CFD Letters*, **14**(6), 102–114. https://doi.org/10.37934/cfdl.14.6.102114

Ghasem Abbasi
Orcid number: 0000-0002-0177-8557
Department of Mathematics
Qazvin Branch, Islamic Azad University
Qazvin, Iran
Email address: Gh.Abbasi@iau.ac.ir

Soheila Khishtandar
Orcid number: 0000-0002-7876-7290
Department of Industrial Management
Qazvin Branch, Islamic Azad University
Qazvin, Iran
Email address: Soheila.Khishtandar@iau.ac.ir